PERGAMON

International Journal of Heat and Mass Transfer 44 (2001) 2763–2776

International Journal of HEAT and MASS TRANSFER

www.elsevier.com/locate/ijhmt

# Bubbling features from a single artificial cavity

Masahiro Shoji *, Yuto Takagi

*Department of Mechanical Engineering, The University of Tokyo, 7-3-1 Hongo, Bunkyo-ku, Tokyo 113-8656, Japan*

Received 3 March 2000; received in revised form 30 June 2000

**Abstract**

Dynamical behavior of nucleation sites is one of the critical factors in boiling, but not many researches, especially experimental, exist in this area. In this paper, a single artificial cavity was manufactured on a thin Cu plate and was heated by laser in a saturated water pool. Conical, cylindrical and reentrant cavities were tested. Conical cavities showed highly intermittent bubbling with large temperature fluctuations, requiring high superheat. Reconstructed phase map from temperature–time series revealed the nonlinear behavior of bubbling, and analysis showed strong possibility of low dimensional chaos. Cylindrical cavities showed continuous bubbling from low superheat with small temperature fluctuations and return map was constructed from bubbling interval. Reentrant cavities showed similar but slightly more complicated behavior than those of cylindrical cavities. © 2001 Elsevier Science Ltd. All rights reserved.

## 1. Introduction

Researches concerning boiling phenomena have been carried on for more than 50 years throughout the world, mainly because of high heat transfer efficiency and thus, strong industrial needs of applications. Vast numbers of sets of correlation and empirical results have been presented and utilized, such as Rohsenow correlation [1], Katto correlation [2] etc. These researches were carried out mainly based on practical needs, presenting rather simple and functional results. But at the same time, mechanism of the phenomena has often been oversimplified or ignored due to complicity of the phenomena.

Boiling phenomena are usually discussed based on boiling curve, which is a log–log plot of space-time averaged wall superheat and space-time averaged wall heat flux. Great number of models and theories proposed in the past few decades were, in many cases, based on the boiling curve, leading to rather simple results using averaged and statistical values for parameters (such as bubbling frequency and cavity distribution). But on the other hand, boiling is a highly complicated spatio-temporal phenomenon, including phase change, turbulent flow and two-phase flow. It is a phenomenon that shows apparently a random and complicated behavior, in which several elements such as nucleation site characteristics or bubble interactions are nonlinearly combined. Thus it has not been an easy task to strictly and theoretically follow all the dynamics and interactions working in the system.

It is only recently that nonlinear chaotic theories have been started to be applied to boiling researches. Ellepola et al. [3] have done a boiling experiment on a thin stainless plate. They measured a temporal temperature distribution of the plate using liquid crystal and carried out nonlinear analysis both on experimental results and calculated results from models. It is considered in these researches that boiling phenomena are a spatio-temporal chaotic system, and their model indeed did support this idea. But it is generally quite difficult to extract nonlinear figures from experimental results, since experiments exhibit nonlinearly combined effects from various elements. In this sense, it seems to be favorable to simplify the experimental system as much as possible and try to extract characteristics of one of the elements consisting of boiling phenomena.

Bubbling behavior of nucleation sites is one of the critical elements in boiling phenomena. Many theoretical and mostly statical discussions [4], such as about stability criteria of a cavity as a nucleation site, can be seen in the past literatures. Recently, Kenning [5] has

* Tel.: +81-3-5800-6987; fax: +81-3-5800-6987.

*E-mail addresses:* shoji@photon.t.u-tokyo.ac.jp (M. Shoji), yuto@photon.t.u-tokyo.ac.jp (Y. Takagi).

0017-9310/01/$ - see front matter © 2001 Elsevier Science Ltd. All rights reserved.
PII: S0017-9310(00)00300-8

**Nomenclature**

| | |
|---|---|
| $C(r)$ | correlation integral |
| $d$ | correlation exponent |
| $D$ | cavity entrance diameter |
| $D_c$ | correlation dimension |
| $r$ | distance in phase space |
| $\Delta t_n$ | bubble departure interval between $n$th bubble and $n+1$th bubble |

proposed that reentrant type cavities have structures which might lead to complicated bubbling behavior. Looking into past experimental researches, Sluyter et al. [6] have manufactured reentrant type cavities on a stainless plate and conducted a boiling experiment. But not many experimental reports are available in this area, due to the difficulty of manufacturing or specifying the geometry and the location of a single cavity.

In this past decade, there was a remarkable advance in micro-scale machining, which threw light on the problem of manufacturing a single micro-scale sized cavity. Especially, micro-electrical discharge machining technique is unique in a sense that it is possible to specify the size and the depth and manufacture a micro-scale sized cylindrical hole.

The present study aims to experimentally characterize bubbling behaviors of three types of cavities, of which are conical, cylindrical and reentrant. Temperature just below the cavity is measured by radiation thermometer, and bubbling behavior is recorded by a high-speed video camera. Series of nonlinear analysis will be carried out for temperature–time series and succeeding bubble departure interval, to reveal nonlinear characteristics in bubbling mechanism.

## 2. Experimental setups

### 2.1. Artificial cavity

In this study, three types of artificial cavities were tested as nucleation sites. They were respectively manufactured on the center of a 0.1 mm thick 10 mm diameter Cu disk surface. Roughness of Cu surface was of the order of 1 μm. Treated cavity types were conical, cylindrical and reentrant. Conical type cavity was produced by pressing a diamond bit on the surface of thin Cu plate via micro-hardness meter. Cylindrical type cavity was produced by the use of micro-electrical discharge machining. Reentrant type cavity was produced by pressing a diamond bit on Cu surface placing a conical cavity and manufacturing a small pit inside the conical cavity by micro-electrical discharge machining. Five different sizes and types of cavities were arranged as shown in Table. 1. The SEM photos and schematic views of cavities are shown in Fig. 1.

Table 1
Size variation of artificial cavities

| Cavity type | Cavity diameter (μm) | Cavity depth (μm) |
|---|---|---|
| Conical | 50 | 30 |
| Conical | 100 | 50 |
| Cylindrical | 50 | 30 |
| Cylindrical | 100 | 50 |
| Reentrant | 100 | 50 |

### 2.2. Apparatus

Cu disk with an artificial cavity was set inside the boiling chamber filled with distilled water. In the experiment, vicinity of the manufactured cavity was heated by Nd–YAG laser irradiation ($\lambda = 1064$ nm) from the bottom side of the Cu disk. The bottom surface of the Cu disk was black oxide finished to increase absorptivity of the input laser and emissivity from the surface. Temperature fluctuations just under the artificial cavity were recorded by radiation thermometer with spatial resolution of 600 μm, temperature resolution of 0.08 K and time resolution of 3.0 ms. The corresponding bubbling status was recorded by a high-speed video camera with the rate of 1297 frames/s. In this way, it was possible to measure temperature–time series of cavity vicinity without any physical contact to the Cu disk surface. A simplified illustration of a vicinity of a cavity is shown in Fig. 2. The power of Nd–YAG laser was controlled to vary the heat input to the Cu disk surface, and was monitored by photo detector throughout the experiment. Working fluid was distilled water at atmospheric pressure under saturated pool boiling condition. Acrylic fence was set inside the chamber to avoid effect of bubbling from auxiliary heater, which was activated during the experiment to maintain saturated boiling condition. Schematic view of the whole experimental setup is shown in Fig. 3.

## 3. Results

### 3.1. Conical type cavities

#### 3.1.1. Temperature–time series

Conical type cavities required rather high superheat to maintain bubbling, and showed strong intermittence

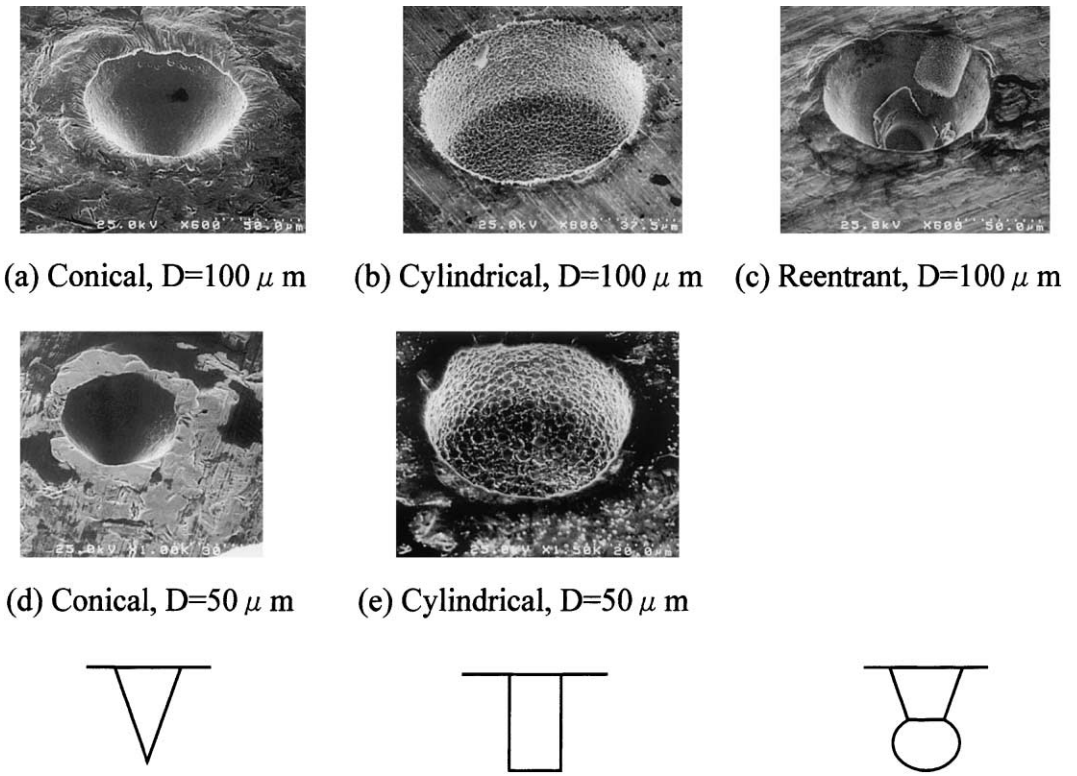


Fig. 1. Variation of artificial cavities.

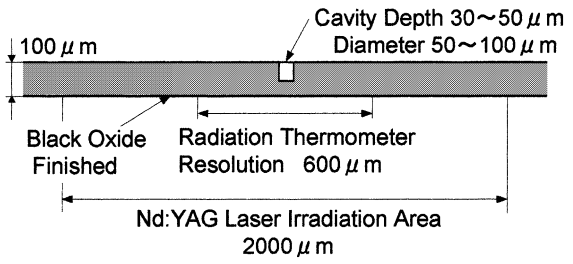


Fig. 2. Heated surface.

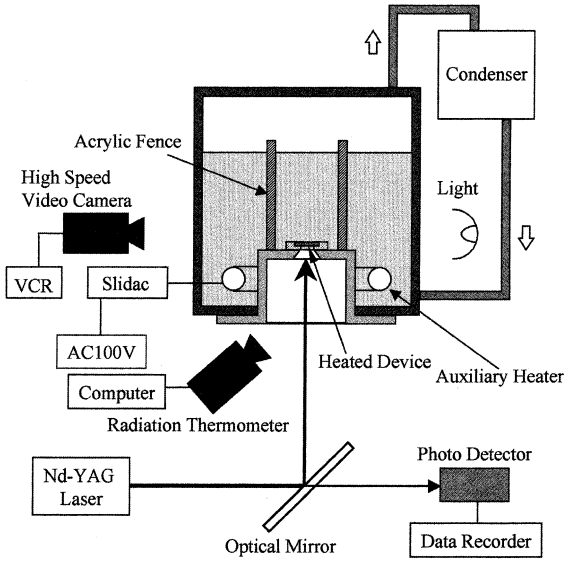


Fig. 3. Schematic view of experimental apparatus.

both in its temperature–time series and bubbling phenomena itself, suggesting rather low ability of holding bubble nuclei. Temperature–time series Fig. 4 consisted of large scale triangular waves (for example, period $\tau_1$ in Figs. 4(a-1) and (b-1)), and series of short-term waves with small temperature fluctuations following them (for example, period $\tau_2$ in Figs. 4(a-1), and (b-1)). Period $\tau_1$ corresponds to waiting period while period $\tau_2$ corresponds to bubbling period. The maximum value of large scale triangular waves corresponds to the bubble initiation temperature. These will be discussed in detail afterwards.

Temperature–time series of conical cavities showed big fluctuations compared to other two types of cavities. It can be seen that power increase generally leads to shortening the length of triangular waves (period $\tau_1$, or

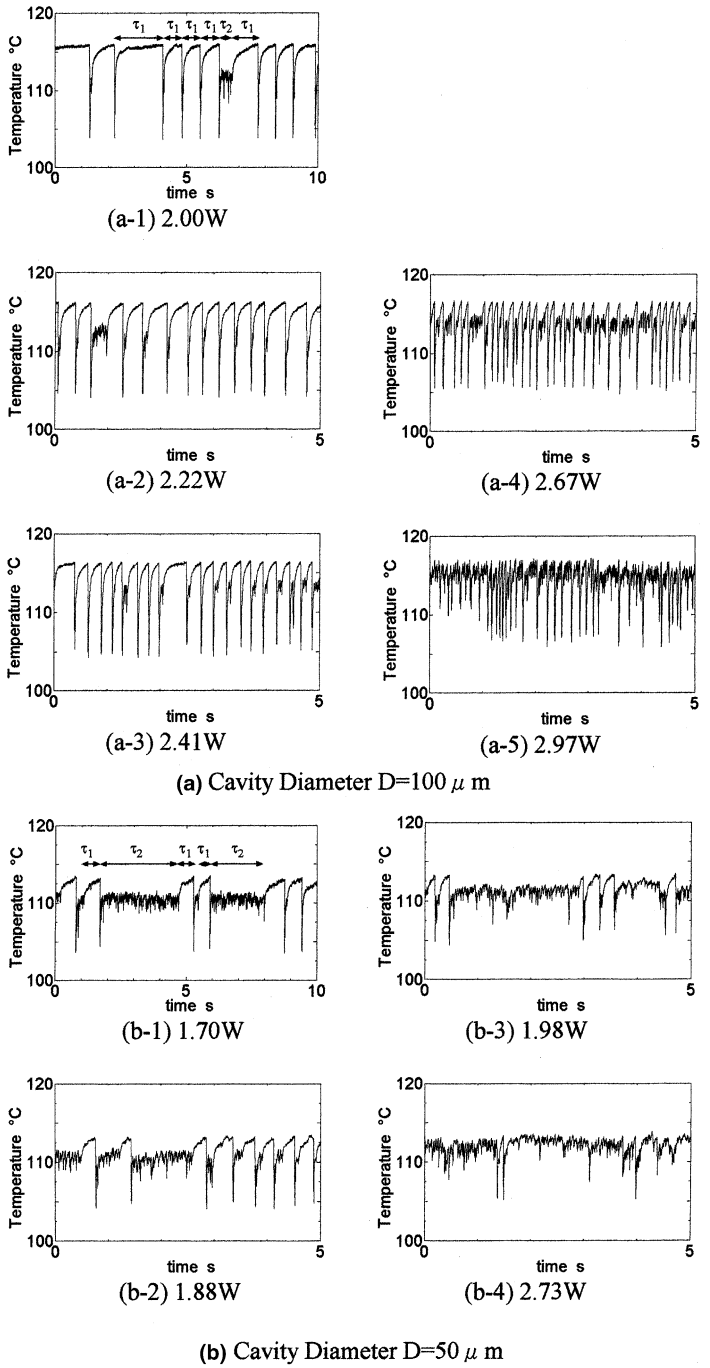


Fig. 4. Temperature–time series of conical cavities (input laser power specified below figures).

waiting period). There was not a big difference in maximum value of triangular waves nor temperature fluctuation amplitude while the input power has been varied. To examine the phenomena in more detail, images from a high-speed video camera were investigated.

*3.1.2. Images from HVC*

Fig. 5 shows images obtained from high-speed video camera recordings. It shows a typical behavior of bubbling from conical cavities. This is a recording right after a waiting period, which was about 100 ms. Fig. 6 is an

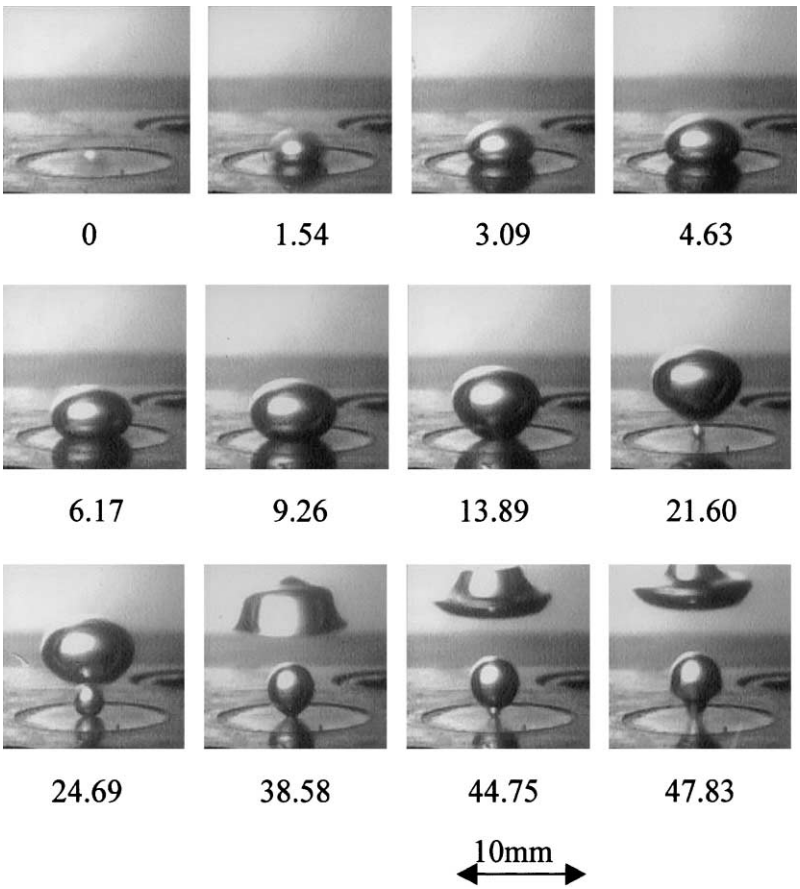


Fig. 5. Bubbling from conical cavity, $D = 100$ μm, all units in ms (input laser power 2.5 W).

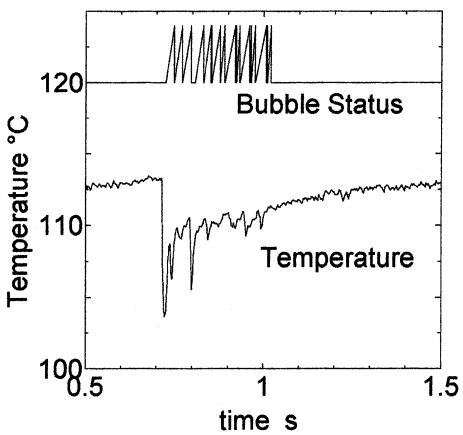


Fig. 6. Temperature–time series and corresponding bubble status (enlarged view of Fig. 4(b-1)).

enlarged view of Fig. 4(b-1) with corresponding bubble status. Saw tooth waveform at the upper part of the diagram represents the bubble status, where the rise in a wave indicates the birth of a bubble, and the drop in the wave indicates the departure of the bubble from the surface. From Fig. 5, we can see the rapid growth of a bubble generated right after a waiting period (let us name this bubble "the first bubble" for simplicity), especially to the horizontal direction.

As this first bubble grows, it can be seen that the three-phase contact line between the bubble and the heated surface is moving outwards rapidly, enhancing phase change at the contact line interface. The rapid movement of the three-phase contact line will remove considerable amount of heat from the heated surface at a very short duration of time (about one-tenth of the whole bubble birth–detachment cycle), and explains the large sudden drop of temperature at the birth of the first bubble in Fig. 6. As a result of this strongly enhanced phase change, size of the first bubble is relatively large.

From Fig. 5, bubbles generated after the first bubble seem to be much smaller than the first bubble, and the directions of their growths are rather isotropic and in spherical shapes. This can be explained by the fact that flow induced by preceding bubble exists around the

growing bubble, and thus the bubble tends to grow upwards, allowing only small movement of the three-phase contact line. This means that phase change at the interface in these cases is not as enhanced as it was in the case of the first bubble, allowing only small temperature drop at their birth. Bubble birth temperature is lower

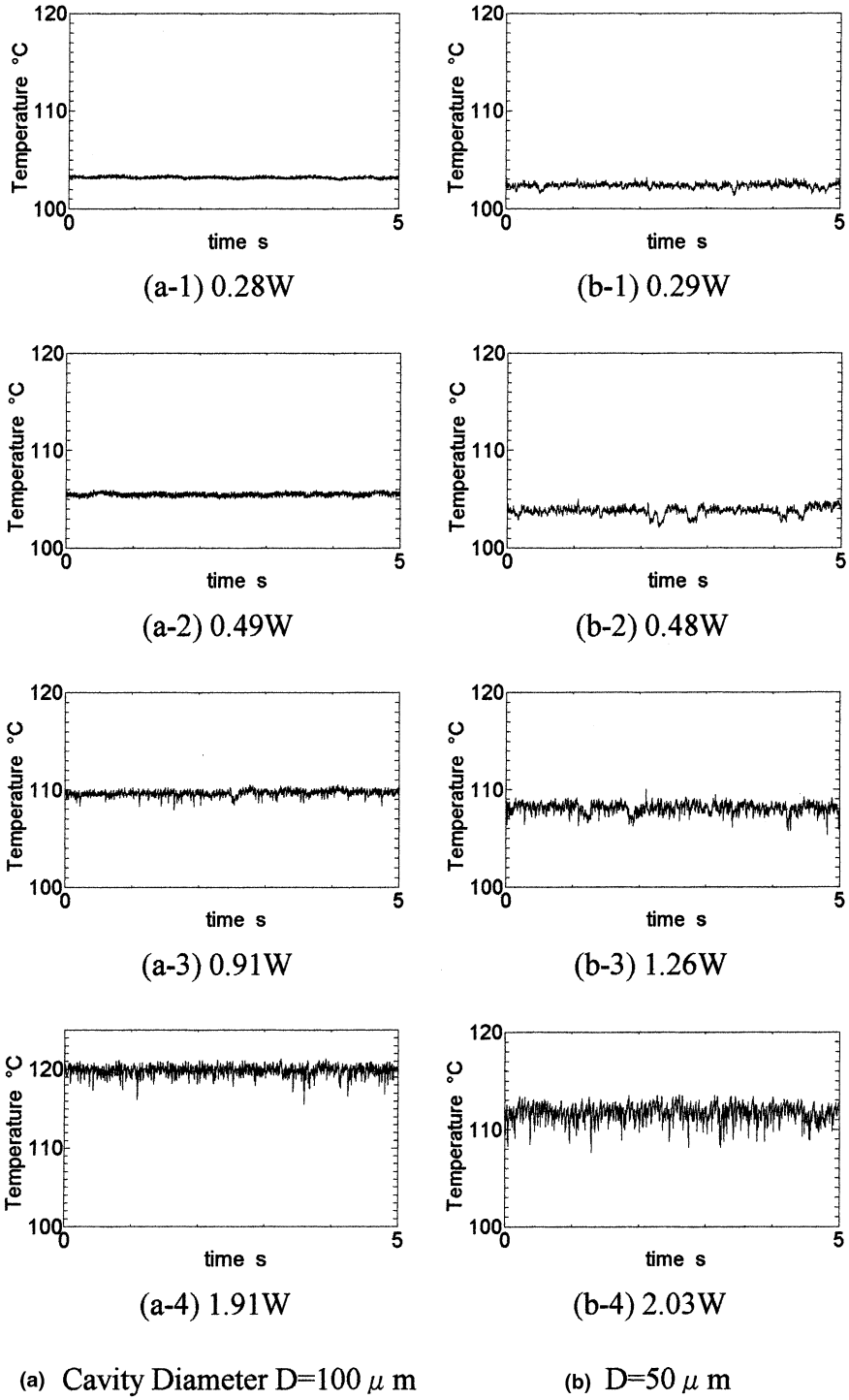


Fig. 7. Temperature–time series of cylindrical cavities (input laser power specified below figures).

than that of the first bubble, presumably because the initial gas–liquid interface exists at the entrance of the cavity. These bubbles show a rather complicated behavior such as pulling in following bubbles and coalescing together and continuing bubbling during period $\tau_2$ (bubbling period) in Fig. 4. Temperature around the cavity basically does not rise or rises quite slowly during this period, because of totally enhanced heat transfer due to bubbling.

After series of continuous bubbling after the first bubble, bubbling suddenly ceases and waiting period starts again. It can be assumed that the initial position of gas–liquid interface moved from the entrance of the cavity to inside the cavity due to some reason. In the case of conical cavity, the curvature of the gas–liquid interface increases as the interface moves into the cavity, and consequently requires higher bubble initiation temperature. Temperature at the vicinity of the cavity gradually rises during waiting period, till it reaches the bubble initiation temperature (the maximum value of saw tooth like waves in Fig. 4). After this waiting period, a large bubble like the first bubble appears again.

### 3.2. Cylindrical type cavities

#### 3.2.1. Temperature–time series

Cylindrical type cavities showed stable and continuous bubbling from rather low superheat, and almost no waiting period observed. Stable bubbling was observed at a superheat about 10 K lower than the case of conical

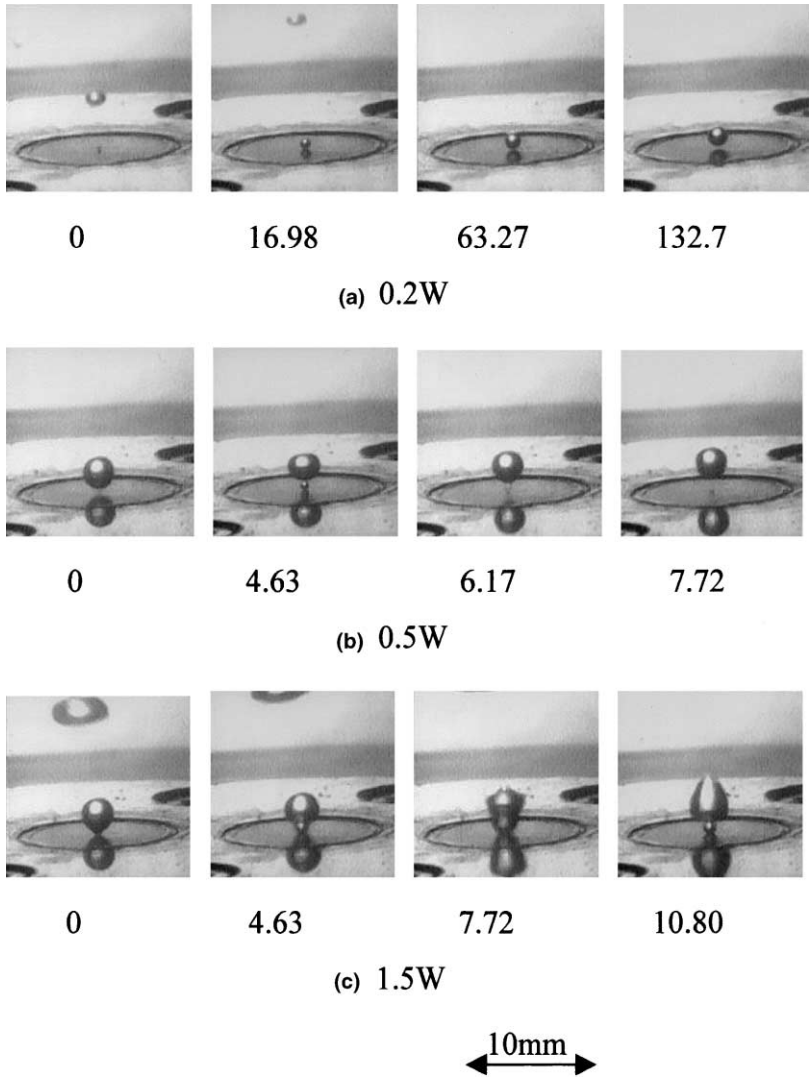


Fig. 8. Bubbling from cylindrical cavity, $D = 50$ μm, units in ms.

cavities. This fact suggests that cylindrical cavities have high ability of holding bubble nuclei. Temperature fluctuations were very small. Though bubbling was observed visually, no obvious sign of bubbling could be seen in temperature–time series, especially at low superheat (see Fig. 7).

*3.2.2. Images from HVC*

Fig. 8 shows images obtained from high-speed video camera recordings. Generally, sizes of bubbles generated from this type of cavities are much smaller than those of conical cavities. Since there is no waiting period, flow induced by the preceding bubble continuously exists. By this flow, a generated bubble tends to grow upwards, and thus the three-phase contact line under the bubble stays at the initial position without moving outwards. Phase change at the interface is not as enhanced as the case of conical cavities, naturally leading to smaller bubbles generated.

Fig. 8(a) shows behavior of a bubble when input laser power is relatively low (0.2 W). In this range, bubble birth and departure seems to be periodic, and shapes of bubbles are almost perfectly spherical. No interactions between bubbles can be seen, and no coalescence can be seen either.

Fig. 8(b) shows behavior of bubbles when input laser power is in intermediate range (0.5 W). In this range, bubbles start to coalesce with each other, in a form such that preceding bubbles pull in following bubbles. Considerable deformation in shapes of bubbles cannot be seen in this range yet.

Fig. 8(c) shows behavior of bubbles when input laser power is relatively high (1.5 W). In this range bubbles coalesce together frequently and big oscillations and deformations in shapes and bubbles are often seen.

*3.3. Reentrant type cavity*

*3.3.1. Temperature–time series*

Reentrant type cavity showed stable and continuous bubbling from rather low superheat, very similar to those of cylindrical type cavities. Almost no waiting period was observed. Quite small temperature fluctuations were observed, and it was difficult to distinguish signs of bubbling from temperature–time series (see Fig. 9).

*3.3.2. Images from HVC*

Fig. 10 shows images obtained from high-speed video camera recordings. Images of bubbling were very similar to those of cylindrical cavities, only showing slight difference in correspondence between the laser input power and events such as coalescence between bubbles. Fig. 10(a) shows snapshots of a bubble when laser power is relatively low (0.2 W). Bubble birth and departure are periodic, and shapes of bubbles were almost perfectly spherical. No coalescence was seen. Fig. 10(b) shows behavior of bubbles when input laser power is in inter-

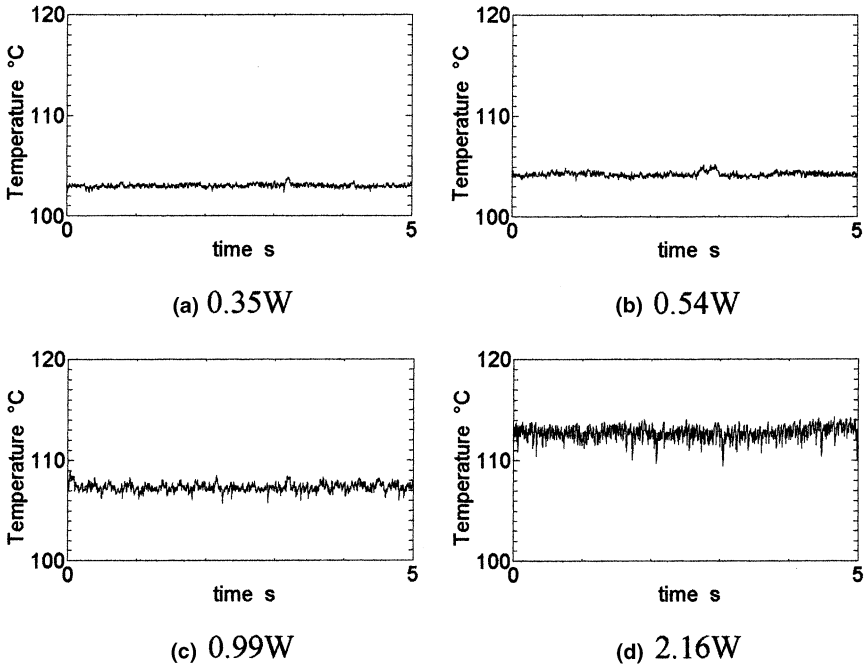


Fig. 9. Temperature–time series of reentrant cavity, $D = 100$ μm (input laser power specified below figures).

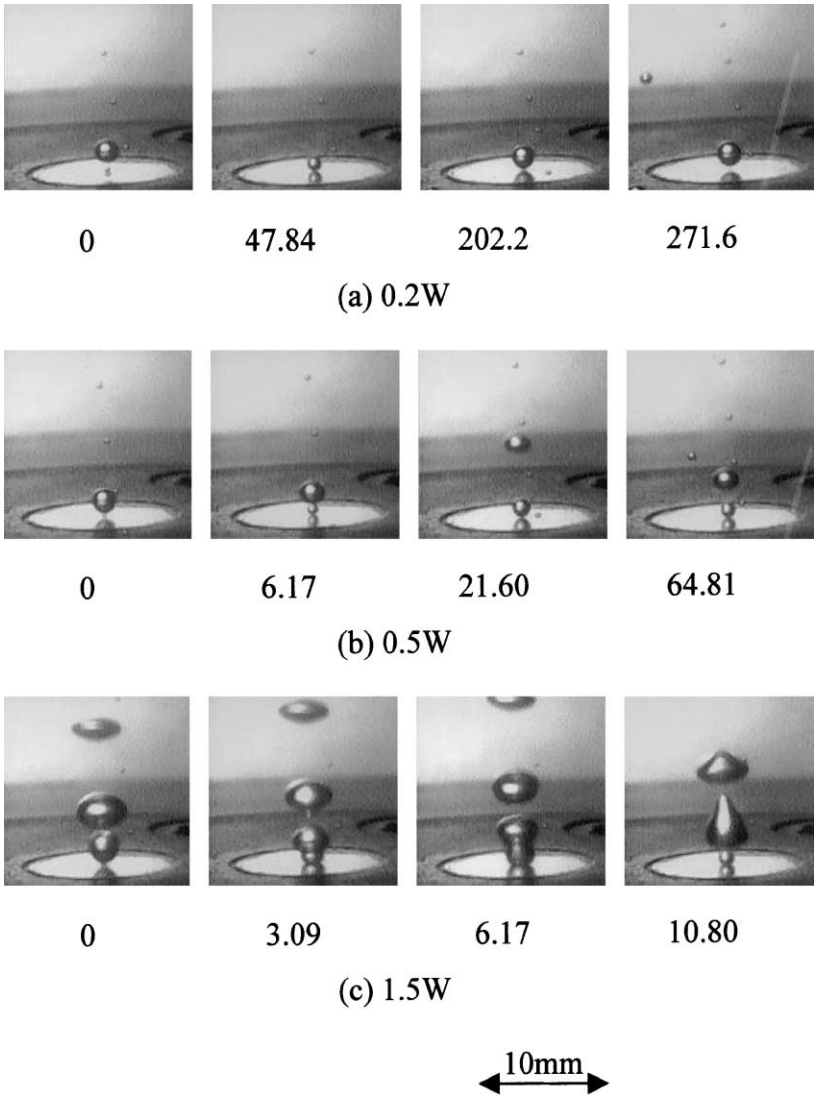


Fig. 10. Bubbling from reentrant cavity, $D = 100$ μm, units in ms.

mediate range (0.5 W). Preceding bubble starts to pull in a following small bubble. Fig. 10(c) shows views of bubbles when input laser power is relatively high (1.5 W). Bubbles coalesce together frequently and large oscillations and deformations in shapes of bubbles were seen.

## 4. Nonlinear analysis

### 4.1. Conical cavities

#### 4.1.1. Phase maps

Temperature–time series of conical type cavities can be characterized by two different scale waveforms: large scale triangular waves, which correspond to the waiting periods and the birth of the first bubble, and short-term small scale waves, which correspond to series of bubbling following the first bubble. In order to get better understanding of the phenomena, reconstruction of phase space from temperature–time series was carried out (see Fig. 11). This was done in a manner of embedding space method, following Taken's embedding theorem [7]. Takens proved that a time series of a single variable measured for a given system in steady state can be used to reconstruct the trajectory of the system by means of a procedure called embedding. Variable sets were chosen as $\{x(t),\ x(t+\tau),\ x(t+2\tau)\}$ for three-dimensional embedding, where $\tau$ was chosen as 12 ms, referring to the first local minimum of mutual

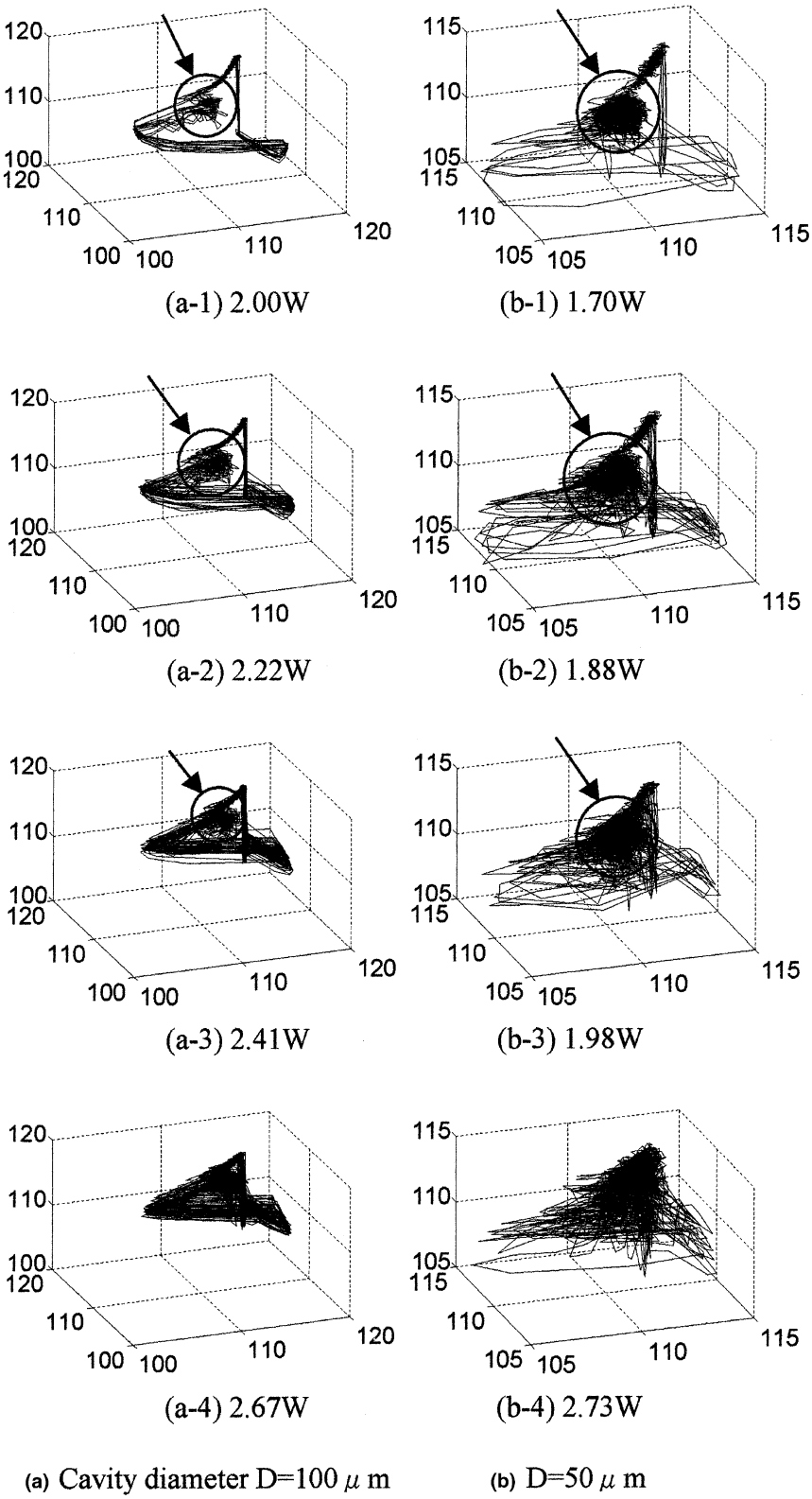


Fig. 11. Reconstructed phase map for conical cavities, units in °C.

information of the time series [8]. Theoretically $\tau$ can be any value, but for experimental data, some methods to determine $\tau$ have been suggested. First local minimum of mutual information is one of the commonly used values for embedding delay time in reconstruction of phase space.

As can be easily seen at the lower laser power range, each attractor consists of relatively large triangle-like trajectories and relatively small tangled ball-like trajectories at the upper right of the phase map (pointed out in Fig. 11(a-1)). Large triangle-like trajectories represent long-term, saw tooth-like waves in temperature–time series, where small ball-like trajectories represent short-term, small-scale fluctuations in temperature–time series. As the laser input increases, trajectories begin to tangle and show rather complicated aspect of the phenomena. But even then, there seems to be a structure there, consisting of two different sized trajectories.

Comparing the case where cavity diameter is 100 μm with the case of 50 μm, we can see that there is a difference in density of trajectories. In the case of $D = 100$ μm, the outside triangle-like trajectories seem to have stronger attracting force, whereas in the case of $D = 50$ μm, the inner-side ball-like trajectories seem to have stronger attracting force. This can be understood if we take a careful look at the transient temperature, where in the case of $D = 100$ μm, long-term, saw tooth-like waves are more frequently seen than those in the case of $D = 50$ μm. This fact implies that once the bubbling begins, cavities with smaller entrance diameter are more stable than cavities with larger entrance diameter. Further nonlinear analysis on this phase map is carried out in the next section.

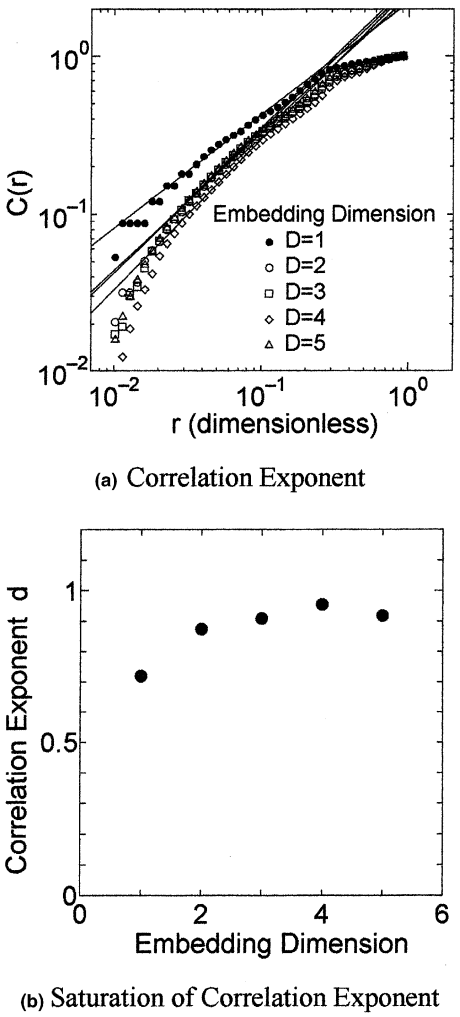


Fig. 12. Correlation dimension, conical cavity $D = 100$ μm, laser power 2.41 W.

*4.1.2. Nonlinear properties*

Correlation dimension and Lyapunov exponent are both well-known properties representing nonlinear characteristics of shape of trajectories or attractors. Correlation dimension is one of the generalized

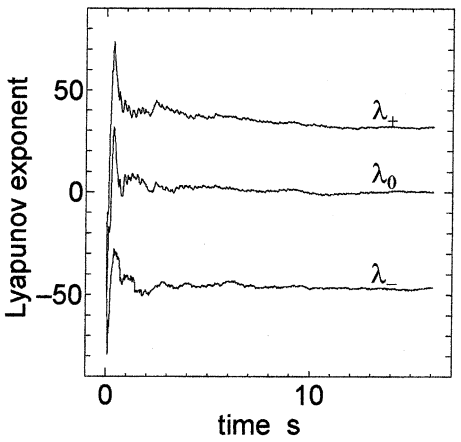


Fig. 13. Lyapunov exponent, conical cavity $D = 100$ μm, laser power 2.41 W.

Table 2
Nonlinear properties of attractors, conical cavities

| Cavity diameter | Input laser power (W) | Correlation dimension | Maximum Lyapunov exponent |
|---|---|---|---|
| 50 μm | 1.69 | 0.94 | 4.9 |
| | 1.88 | 1.80 | 10.3 |
| | 1.98 | 2.28 | 12.5 |
| | 2.73 | 2.31 | 14.8 |
| 100 μm | 2.00 | 0.49 | −0.3 |
| | 2.22 | 0.60 | 10.0 |
| | 2.41 | 0.95 | 31.9 |
| | 2.67 | 1.36 | 38.5 |

dimensions that can take fractional values. It describes the quantitative strangeness of unfamilar geometric structure of trajectories in phase space. Lypunov exponent is a quantitative measure that represents sensitivity to changes in initial conditions. It is a barometer, which indicates the extent of a loss of information or a loss of predictability. When the largest Lyapunov exponent is positive while the sum of all Lyapunov exponents is negative, and when the correlation dimension takes a fractal value, there is a strong possibility of "chaos" in the system. Correlation dimension also specifies the minimum independent variables needed to define the system.

Correlation dimension is derived as follows. First, correlation integral $C(r)$ is calculated on each embedded dimension phase space, respectively.

$$C(r) = \lim_{N\to\infty} \frac{1}{N^2} \begin{pmatrix} \text{number of pairs } (i,j) \\ \text{with distance } s_{ij} < r \end{pmatrix}. \quad (1)$$

It has been found that for $r \to 0$,

$$\lim_{r\to 0} C(r) = ar^d \quad (2)$$

If we plot $C(r)$ versus $r$ in a log–log plot, then the slope of the line will be the correlation exponent $d$. If this correlation exponent saturates as the embedding dimension is increased, the saturated exponent $D_c$ is called as the correlation dimension. Fig. 12(a) shows one example of $C(r)$ versus $r$ in a log–log plot, and Fig. 12(b) shows saturation of correlation exponent.

Example of a result of calculating Lyapunov exponent is shown in Fig. 13. In this case, we can see that the Lyapunov exponents have converged to certain values, and the sum of all exponents being negative.

Table 2 shows calculated correlation dimensions and maximum Lyapunov exponents from temperature–time series of conical cavities. In all cases, Lyapunov exponents converged to certain values and their sums were

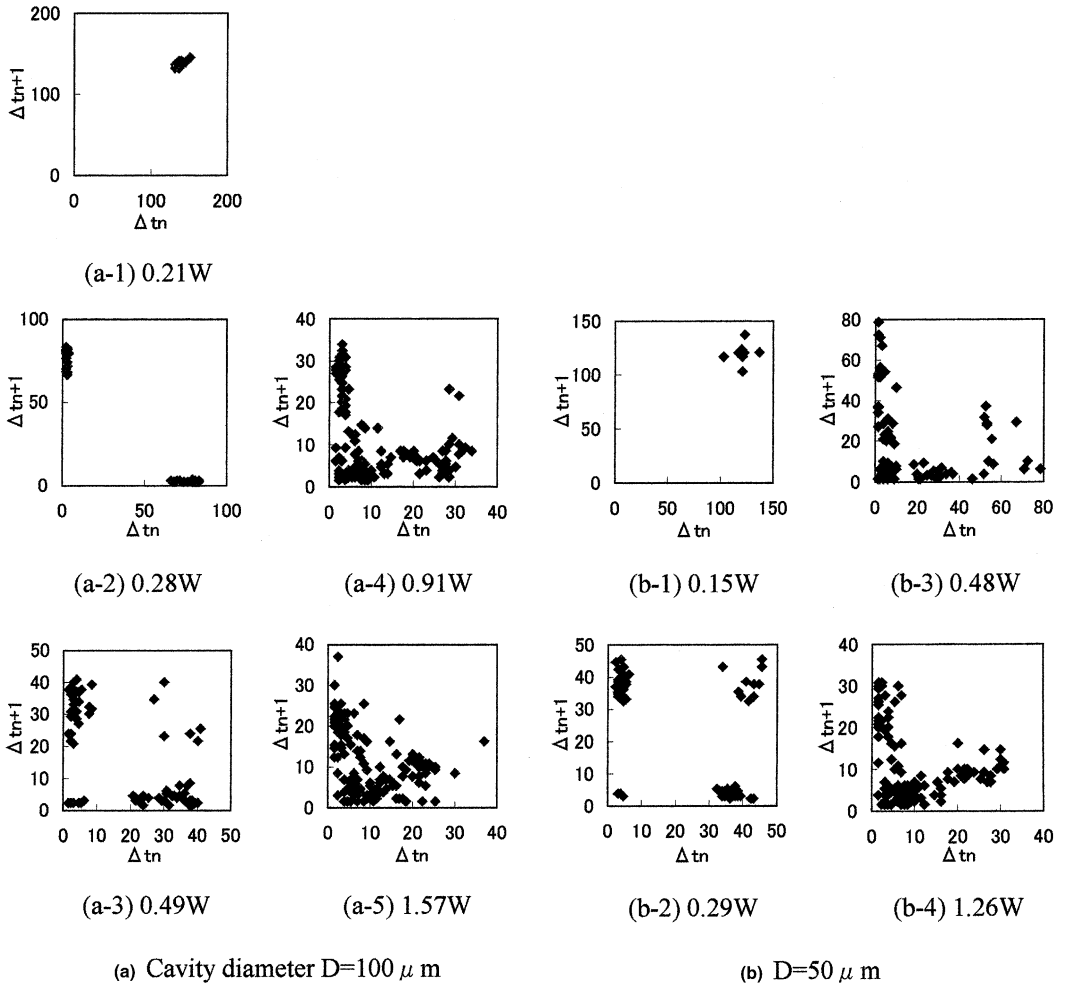


Fig. 14. Reconstructed return map for cylindrical cavities, all units in ms.

negative, supporting the validity of calculation procedure. Correlation dimensions turned out to be extremely low values, some of them below one. These results strongly suggest the existence of low dimensional chaos in this system, and a possibility of sufficiently modeling this system by very few variables. It might be possible to extremely simplify this system, and still construct a model that sufficiently holds nonlinear characteristics of the original system. For example, a simple spring-mass system could be tried, or other simple assumptions could be made such as to treat shapes of bubbles as perfect spheres.

### 4.2. Cylindrical cavities – return maps

Since there were only small fluctuations in temperature–time series, it was impossible to reconstruct phase map in the same manner as the case of conical cavities. Instead, return map was constructed from succeeding bubble departure intervals, obtained from high-speed video camera recordings. Return map is a useful tool to diagnose relations between succeeding happening events, constructed in the following manner. Series of departure time interval between bubbles were taken, and the interval between $n$th bubble and $n+1$th bubble, $\Delta t_n$, were plotted on the $x$-axis, while the interval between $n+1$th bubble and $n+2$th bubble, $\Delta t_{n+1}$, plotted on $y$-axis, successively. In this way, we can visually know the effect of a certain bubble departure interval on the next bubble's departure. At the same time, periodic or quasi-periodic phenomena can easily be recognized by cluster of points in the map.

Fig. 14 shows return maps reconstructed from high-speed video camera recordings for cylindrical type cavities. At the range where input laser power is extremely low, only periodic bubbling can be seen (see Figs. 14(a-1) and (b-1)). As input laser power is increased, coalescence of bubbles takes place, leading to very short bubble departure time intervals like Fig. 14(a-2). At intermediate input laser power range, it is possible to distinguish between bubbles departed with coalescence and without coalescence (see Figs. 14(a-3) and (b-2)). At rather high laser power range, it is difficult to distinguish bubbles departed with or without coalescence, and bubble departure intervals range in broad values. But still, the distribution is not random, showing some structure or function between the succeeding bubble departure intervals.

This fact implies the possibility of existence of deterministic chaos in this system. Further nonlinear

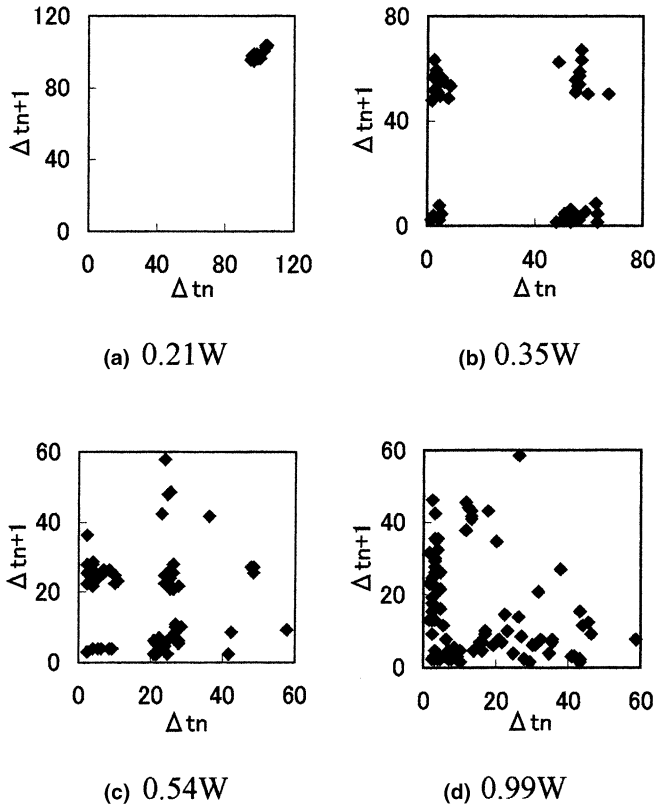


Fig. 15. Reconstructed return map for reentrant cavities, all units in ms.

analysis is desired, but numbers of data points were definitely not enough to move further on. Some other methods to measure bubble departure interval are expected in the future.

### 4.3. Reentrant cavities – return maps

Return maps for reentrant type cavities were reconstructed in exactly the same manner as the case of cylindrical type cavities (see Fig. 15). Basically, return maps showed same trends as those of cylindrical cavities. Bubbling started single periodic mode, showing short-term bubbling due to coalescence between bubbles as the input laser power was increased. But at intermediate range (see Fig. 15(c)), return map showed rather strange form. It might be emergence of period 3, but numbers of data points were not enough to move on to further discussions. At rather high input laser power range, return map was very similar to that of cylindrical type cavities, indicating the possibility of deterministic chaos.

## 5. Conclusions

Three different types of artificial cavities were manufactured, and boiling experiments were carried out to reveal bubbling characteristics depending on geometry of cavities. While conical cavities showed intermittent bubbling with large temperature fluctuations and required rather high superheat to maintain bubbling, cylindrical and reentrant cavities showed continuous and stable bubbling from rather low superheat.

Series of nonlinear analysis were carried out and correlation dimensions, Lyapunov exponents were calculated from temperature–time series of conical cavities. Rather low correlation dimensions and positive maximum Lyapunov exponents were obtained, suggesting the existence of low dimensional chaos in this system. Return maps were constructed for cylindrical cavities and reentrant cavities from bubble departure intervals, revealing the structure of the phenomena and indicating the possibility of deterministic chaos.

## References

[1] W.M. Rohsenow, A method of correlating heat transfer data for surface boiling of liquids, Trans. ASME 84 (1962) 969–976.
[2] Y. Haramura, Y. Katto, A new hydrodynamic model of critical heat flux, applicable widely to both pool and forced convective boiling on submerged bodies in saturated liquids, Int. J. Heat Mass Transfer 26 (1983) 389–399.
[3] J. Ellepola, D. Kenning, Nucleation site interactions in pool boiling, in: Proceedings of the Second European Thermal Sciences and 14th UK National Heat Transfer Conference, Rome, 1996.
[4] K. Mizukami, Stability of bubble nuclei and nucleation in isothermal liquid, Rev. Kobe Univ. Mercantile Marine 2 (27) (1979).
[5] D.B.R. Kenning, Wall temperature variations and the modeling of bubble nucleation sites, in: Proceedings of the Pool and External Flow Boiling Conference, 1992, 105–110.
[6] W.M. Sluyter, C.A.C. Slooten, A.K. Chesters, The departure size of pool-boiling bubbles from artificial cavities at moderate and high pressures, Int. J. Multiphase Flow 17 (1) (1991) 153–158.
[7] F. Takens, Detecting strange attractors in turbulence, Lect. Notes Math. 898 (1981) 366–381.
[8] A.M. Fraser, H.L. Swinney, Independent coordinates for strange attractors from mutual information, Phys. Rev. A 33 (2) (1986) 1134–1140.